SIMULATION OF HYDRAULIC FRACTURING IN ROCKS

A.GOLSHANI[1] and T.TRAN-CONG[2]

[1]*Faculty of Engineering and Surveying, University of Southern Queensland, Toowoomba, QLD, Australia*
golshani@usq.edu.au

[2]*Faculty of Engineering and Surveying, University of Southern Queensland, Toowoomba, QLD, Australia*

Abstract

To investigate the breakdown pressure and the energy transferred to the surrounding rock, numerical simulations of circular boreholes under internal hydraulic pressure are carried out. For this purpose, a micromechanical continuum damage model proposed by Golshani et al. [1] is used. The simulation results show that the borehole breakdown pressure and the energy transferred to the surrounding rock are dependent on the mechanical properties of the rock, borehole size and far-field confining stresses. Although the energy transferred to the surrounding rock increases with increasing borehole size, the borehole breakdown pressure decreases. The analysis also shows that breakdown does not occur even if a crack initiated at a borehole wall. In fact, the breakdown occurs when the crack growth becomes unstable. In other words, breakdown pressure appears to correspond to the onset of unstable crack growth.

1. Inroduction

Stresses are applied inside the boreholes either to produce deformations in order to determine the modulus of the rock or to induce fractures [2]. Hydraulic fracturing is one of the techniques used to stimulate the production of oil or gas in reservoirs. This technique involves pumping a fluid under pressure into a borehole. This pressurized fluid introduced into the borehole produces stress concentration in the surrounding rock causing the development of fractures. Furthermore, hydraulic fracturing is the common method for stress measurement in geotechnical engineering application. Breakdown pressure i.e., the pressure at which fracturing occurs, is regarded as a function of the state of stress. In fact, attention is focused on the prediction of the borehole breakdown pressure and is usually the only parameter available to evaluate the operation [3]. However, the energy transferred to the rock during pressurization of the borehole can be considered as another parameter for the evaluation of the operation.

Energy can be stored in or released from the rock medium in the vicinity of a borehole subjected to internal pressure. If the internal energy exceeds the limit that the material can withstand, the energy release will occur to re-establish the internal energy level within a tolerable limit. Griffith [4] suggested that a potential relief mechanism is the micro-cracking. According to his theory the excess of energy is dissipated with the growth of microcracks during rock failure.

The energy transferred to the surrounding rock associated with the phenomena occurring in the borehole under breakdown pressure (the energy

requirements for rock fracturing) is given by

$$W = W_s + W_f + W_t + W_c \qquad (1)$$

where W_s, W_f, W_t and W_c represent strain energy (borehole wall deformation), fracture energy, thermal energy (thermal exchange between rock and fluid) and chemical energy (chemical change of the rock due to the interaction with the fluid).

The strain energy is the potential energy stored in the rock under stress and is given by

$$W_s = \frac{1}{2}\int_V \sigma : \varepsilon \ dV \qquad (2)$$

where V is the volume of the rock. σ and ε are the stress and strain in the rock under applied stresses. The symbol (:) stands for the inner product.

The fracture energy is material property of rock and is given by

$$W_f = \frac{K_C^{\ 2}}{E} A \qquad (3)$$

where K_c and E are the fracture toughness and Young's modulus of the rock and A is the area of fracture created.

When the internal energy reaches a critical limit, this level must be reduced by one or more relief mechanisms. As previously explained, the most significant relief mechanism for rocks is microcracking.

The main objective of this paper is to investigate numerically the breakdown pressure and the energy transferred to the rock around a vertical borehole under breakdown pressure by using a micromechanics-based continuum damage model proposed by Golshani et al. [1]. For this purpose three types of rocks i.e., Inada granite, Mount Isa granite and Toowoomba basalt are simulated. The effect of borehole diameter and far-field stresses on the breakdown pressure and the transferred energy will also be discussed. In this study we only consider the effects of borehole wall deformation W_s and the fracture energy W_f in energy calculation and the fluid is restricted from entering the microcracks.

2. Micromechanics-base Continuum Damage Model

In this model, the rock matrix is regarded as an elastic solid with N groups of microcracks distributed at different orientations, and the i-th group is characterized by the microcracks orientation $\theta^{(i)}$, the number density of the microcracks $\rho^{(i)}$, and the average microcracks length $2c^{(i)}$. $\theta^{(i)}$ is the inclination angle of the unit vector $n^{(i)}$, normal to a microcrack, to the global axis x_1(see Figure 1). In the following discussion, "^" indicates quantities in the local coordinate x'_i-axes.

By assuming that microcrack growth occurs in tensile mode I [5-8], the stress intensity factor K_I for a single microcrack with respect to local axes x'_i $(i=1, 2)$ is approximated by

$$K_I = -\sqrt{\pi \ c} \ \sigma'_t \qquad (4)$$

where σ'_t is the tensile stress acting normal to the microcrack surface, and is expressed as:

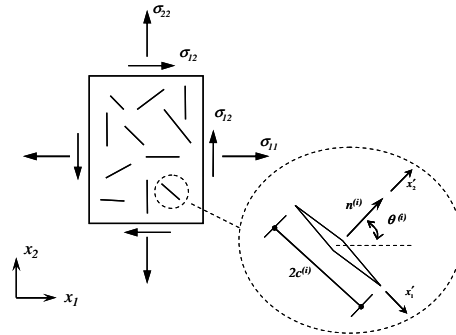$$\sigma'_t = \sigma'_{22} + f(c)S'_{22} \qquad (5)$$

Fig. 1. Rock sample containing many microcracks

It should be noted that the compressive stress is taken to be positive. The first term on the right hand side of Eq. (5) stems from the far field compression, hence it takes a positive value (compression) in a common case. This means that the first term acts as an inhibiting factor for microcracking. The second term is the tensile stress, which is locally generated as a result of

the inhomogeneity of rock and sliding movement on asperities. Following the suggestion by Costin [6], we assume that the local tensile stress increases proportionally to the deviatoric stress S'_{22}, and that $f(c)$ is a proportionality coefficient depending only on half the microcrack length c. It is of particular importance to point out that the local tensile stress must decrease as the microcrack grows. Otherwise, the microcrack would propagate without any limit as soon as the stress intensity factor K_I reaches the fracture toughness K_{IC}. This unsatisfactory situation is easily avoided if the proportional coefficient $f(c)$ is inversely proportional to half the microcrack length

$$f(c) = d / c \qquad (6)$$

where d is a typical length scale of material such as grain size, and is experimentally determined (see Golshani et al., [1]).

The stress-induced microcrack growth takes place in tensile mode I when the following relation is satisfied

$$K_I - K_{IC} = -\sqrt{\pi\ c}\ \sigma'_t - K_{IC} = 0 \qquad (7)$$

Equation (7) was formulated for a single microcrack and the effect of neighbouring microcracks was not considered. In order to evaluate the elastic interaction among neighbouring microcracks, we use the so-called pseudo-traction method developed by Horii and Nemat-Nasser [9-10]. For simplicity, we first consider an infinite plate with two microcracks α and β with lengths $2c_\alpha$ and $2c_\beta$, both of which are subjected to far field stresses (see Fgure 2). This problem is elastically analysed by decomposing it into three sub-problems; i.e. a homogeneous sub-problem and two sub-problems α and β as shown in Figure 2. There is no microcrack in the homogenous sub-problem, which is subjected to the same far field stresses as the original problem (i.e. σ_{11}, σ_{22} and σ_{12}). In the sub-problem α and β, we deal with a single microcrack under zero stresses, individually. The traction-free condition must be satisfied on the surface of the microcracks in the original

problem since the microcracks α and β are assumed to be open. To do this, $-(\sigma'^\alpha_{22} + \sigma'^{P\alpha}_{22})$ and $-(\sigma'^\alpha_{12} + \sigma'^{P\alpha}_{12})$ must be applied to the surface of the microcrack α in the sub-problem α. Here, σ'^α_{22} and σ'^α_{12} are the stresses at the position of microcrack α arising from the far field stresses in the homogenous problem, and $\sigma'^{P\alpha}_{22}$ and $\sigma'^{P\alpha}_{12}$, called pseudo-tractions, stand for the stresses at the position of microcrack α in sub-problem β. That is, the pseudo-tractions are generated by microcrack β through elastic interactions between the microcracks α and β.

The pseudo-tractions are calculated such that all the boundary conditions for the original problem are satisfied

$$\left\{\sigma'^{P\alpha}\right\} = \left[\gamma'^{\alpha\beta}\right]\left(\left\{\sigma'^\beta\right\} + \left\{\sigma'^{P\beta}\right\}\right) \qquad (8)$$
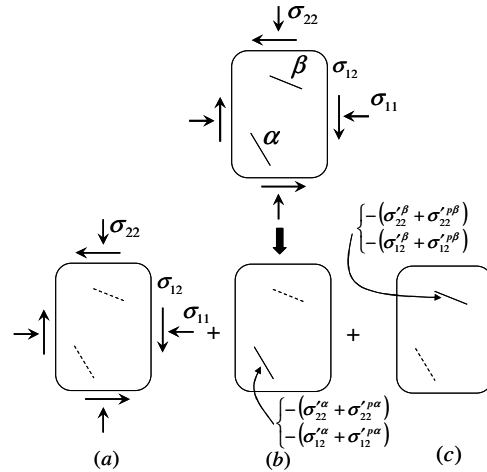

Fig. 2. Decomposition of (a) the original problem into (b) the homogeneous problem and (c) and (d) two sub-problems.

where $\left\{\sigma'^{P\alpha}\right\} = \left\{\sigma'^{P\alpha}_{11}, \sigma'^{P\alpha}_{22}, \sigma'^{P\alpha}_{12}\right\}^T$,

$\left\{\sigma'^\beta\right\} = \left\{\sigma'^\beta_{11}, \sigma'^\beta_{22}, \sigma'^\beta_{12}\right\}^T$,

and $\left[\gamma'^{\alpha\beta}\right]$ is a 3×3 matrix and each element of which is a function of the position vectors x^α and x^β of the centres of microcracks α and β,

their half lengths (c_α and c_β), and the inclination angle between $x_1'^\beta$ and $x_1'^\alpha$. Eq. (8) is tentatively called the consistency equation in the sense that stress boundary conditions are taken into account. If more details are necessary, readers should refer to the papers by Horii and Nemat-Nasser [9-10], Okui et al. [11], and Golshani et al. [1].

Equation (8) was formulated by considering the elastic interaction between two microcracks. In order to deal with more general cases in which a large number of microcracks are involved, the consistency equation (8) can be generalized as an integral equation. Consider N groups of microcracks, we can rewrite Eq. (8) with respect to the global axes x_i ($i=1$, 2), as follows

$$K_I(\sigma', \sigma'^P, c) = \tag{10}$$
$$-\sqrt{\pi c}\left[(\sigma'_{22} + \sigma'^P_{22}) + f(c)\left(\frac{(\sigma'_{22} + \sigma'^P_{22}) - (\sigma'_{11} + \sigma'^P_{11})}{2}\right)\right]$$

It is assumed that the rock matrix remains elastic in the entire process so that the inelastic deformation arises from opening of microcracks. Since the matrix is elastic, the stress-strain relationship is given by:

$$\sigma = D_e : (\varepsilon_t - \hat{\varepsilon}) \tag{11}$$

where D_e is the elastic modulus tensor, ε_t is the total strain tensor and $\hat{\varepsilon}$ is the inelastic strain tensor arising from the opening of microcracks. The inelastic strain caused by the microcracks belonging to the i-th group is obtained in the local axes $x_i'(i=1,\ 2)$ as

$$\hat{\varepsilon}' = \rho^{(i)}\int_{-c}^{c}(n'^{(i)}\otimes[u']^{(i)} + [u']^{(i)}\otimes n'^{(i)})dx' \tag{12}$$

where $n'^{(i)}$ is the unit vector normal to the microcrack, and $[u_2']^{(i)}\left(=(u_2'^+ - u_2'^-)^{(i)}\right)$ is the opening displacement where $u_2'^+$ and $u_2'^-$ are the displacements on the positive and negative sides of the microcrack given as

$$[u_2']^{(i)} = -\frac{\kappa+1}{2G}\sqrt{(c^{(i)})^2 - x_1'^2}(\sigma_t') \quad (|x_1'| \le c^{(i)}) \tag{13}$$

where G is the shear modulus, and κ is the Lame constant [12].

The inelastic strain arising from opening the i-th group microcracks is formulated in terms of the average length of microcracks $2c^{(i)}$, microcracks orientation $\theta^{(i)}$, number density of microcracks $\rho^{(i)}$, and the applied stresses σ[1]. The inelastic strain arising from all microcracks is calculated by summing Eq. (13) with respect to the global coordinate axes

$$\{\hat{\varepsilon}\} = \sum_{i=1}^{N}\left\{\hat{\varepsilon}(c^{(i)}, \theta^{(i)}, \rho^{(i)}, \sigma)\right\} \tag{14}$$

It should be noted that the effect of the elastic interaction among microcracks on the opening displacements and consequently on stress–strain relationship is neglected in Eq. (14). This is a shortcoming. However, this interaction is taken into account in the determination of microcrack lengths through the microcrack growth law Eq. (7).

We now have governing equations for analysing stress-induced behaviour of brittle rock; i.e., microcrack growth law (7), consistency equations (9) and constitutive equations (11). Unknowns are σ, c and σ^p. The initial values of the unknowns are given by solving boundary value problems by using the stress-induced microcrack growth law. They correspond to a state just after the application of a load. Based on the finite element methods, we solved the governing equations on a numerical basis. Three-node triangular elements were used, in each of which the displacement, the interaction stresses and the length of the microcracks belonging to the i-th group are constant.

3. Numerical Simulation

In this study a single borehole in rock medium (3000mm $\times$ 3000mm) was simulated and plane strain condition was assumed. Numerical simulations were carried out for three types of rocks i.e., Inada granite, Mt. Isa granite and Toowoomba basalt to determine the breakdown pressure and the internal energy transferred to the surrounding at failure (using Eqs.1-3).

In finite element modelling, a finer mesh typically results in a more accurate solution.

However, as a mesh is made finer, the computation time increases. A mesh convergence study enables us to obtain an accurate solution with a mesh that is sufficiently dense and not overly demanding of computing resources. Mesh convergence study was performed and we chose a mesh with 195 nodes and 350 elements that satisfies the accuracy requirement of a minimum computational cost (Figure 3).
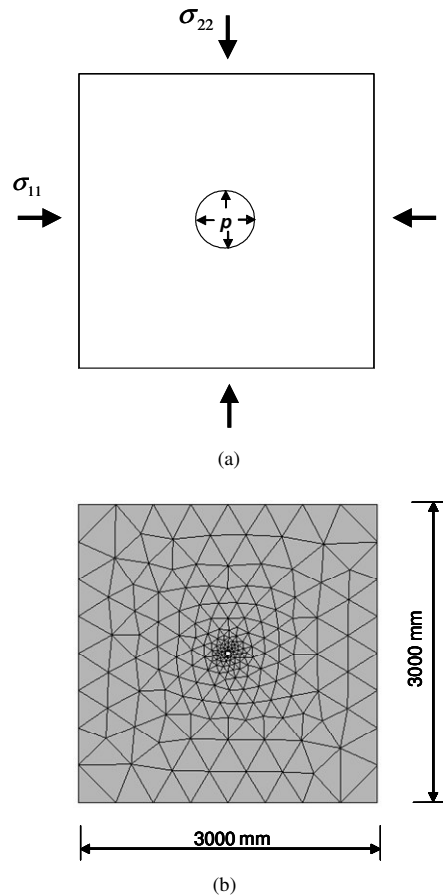

(a)

(b)

Fig. 3. (a) A region with a hole inside under pressure of p (b) Finite element mesh (not to scale)

3.1. *Inada Granite, Mt. Isa Granite and Toowoomba Basalt*

Inada granite is biotite granite from a quarry in Kasama, Ibaraki, Japan. Inada granite consists of coarse to medium grains of quartz, feldspar and biotite. The mean grain size of Inada granite is about 2.0 mm [13]. From earlier study the mechanical and mineralogical characteristics of Inada granite are known: Inada granite elastic properties are Young' modulus $E = 73$ GPa and Poisson's ratio $v = 0.23$. Fracture toughness and length parameter for Inada granite were chosen as $K = 2.5$ MPa$^{1/2}$ and $d = 0.34$ mm. The average length of microcracks and microcrack number density are $c = 0.5$ mm and $\rho = 0.21$ (see Golshani et al., [1]). The uniaxial compression strength and tensile strength of Inada granite were reported as 160 MPa and -7.9 MPa [13].

Table 1. Model parameters used in numerical simulations for Mt. Isa Granite and Toowoomba Basalt

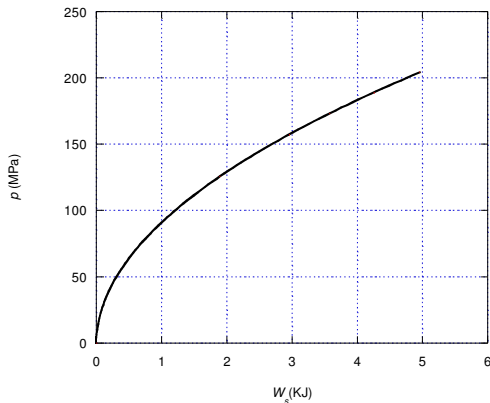| Parameter	Mt. Isa Granite	Toowoomba Basalt
Young's modulus (GPa)	61.4	78.7
Poisson's ratio	0.22	0.25
Fracture toughness (MPa m$^{1/2}$)	1.94	1.88
Initial microcrack length* (μm)	50	12.5
Number density of microcracks*	0.21	0.21
Tensile Strength (MPa)	-10.1	-14.8

* These data are estimates.

Mt. Isa granite occurs in Northwest Queensland, Australia and its grain size is about 0.2 mm (Geoscience report, Australia, 2001). Toowoomba basalt (South-eastern Queensland, Australia) is generally fine-grained, dark grey to black igneous rock. In most cases individual minerals cannot be recognized by the naked eye because of the fine grain size [14]. Basalt is characterized by mineral grain size less than 0.3 mm and for Toowoomba basalt, which is fine-grained basalt, the average grain size is set to 0.05 mm. The input parameter used in the numerical simulation of Mt. Isa granite and Toowoomba basalt are listed in Table 1 where elastic properties and fracture toughness are from experimental tests using samples with 60 mm diameter and 145 mm height.

In crystalline rocks, it is assumed that grain boundaries act as the predominant source of stress concentrating flaws and that the initial microcrack lengths are of the order of the rock grain size [15]. Thus, we can estimate initial microcrack length of Mt. Isa granite and Toowoomba basalt based on their grain size. The microcrack number density of Mt. Isa granite and Toowoomba basalt are not reported and are set to be 0.21 on a tentative basis.

3.2. *Breakdown Pressure and Energy Transferred to the Rock*

The region (3000mm $\times$ 3000mm) with a hole of 50 mm diameter was meshed with 195 nodes and 350 elements (Fig. 3b). Uniform stress was applied inside the borehole with no far-field confining stresses (i.e., $\sigma_{11}=\sigma_{22}=0$) and the energy at failure for Inada granite, Mt. Isa granite and Toowoomba basalt was obtained as 4.5 KJ, 5.7 KJ and 7.3 KJ. The breakdown pressures for theses three types of rocks were 173 MPa, 204 MPa and 255 MPa. The relationship between borehole pressure and transferred strain energy of Mount Isa granite is shown in Fig. 4.

Fig. 4. Relationship between pressure p and strain energy W_s transferred to the surrounding rock.

The tangential stress at the borehole surface was calculated for Inada granite (-62.5 MPa), Mt. Isa granite (-71.4 MPa) and Toowoomba basalt (-85.6 MPa) which significantly exceeds the tensile strength of these rocks obtained experimentally. In other words, the borehole breakdown does not take place even if the largest tangential stress at the borehole reaches the tensile strength of rock. In fact, the breakdown pressure appears to correspond to the onset of unstable microcrack propagation on the borehole wall [16, 17]. Our simulation shows that for Inada granite, at internal pressure of 125 MPa, the length of microcracks in the vicinity of the borehole is about 0.6 mm and during pressurization before breakdown, microcrack growth becomes unstable locally (at internal pressure of 170 MPa, microcrack growth becomes unstable in some areas around the borehole with large cracks of about 3 mm in length) (Figure 5).

Table 2. Breakdown pressure and energy transferred to the surrounding rock at failure

Hole diameter (mm)	Breakdown pressure (MPa)	Energy (KJ)
25	187	2.05
50	173	4.52
75	156	8.08

3.3. *Borehole Diameter*

Borehole sizes of three different diameters of 25 mm, 50 mm and 75 mm in Inada granite were simulated in order to investigate the effect of the borehole size on the breakdown pressure and the The number of elements for these three simulations was 494, 350 and 426, respectively. The results show that borehole breakdown pressure and energy are dependent on the borehole size (Table 2). The borehole breakdown pressure is higher for smaller diameter holes. Morita et al. [17] obtained similar results in the laboratory tests on cubic Berea sandstone (76 cm $\times$76 cm $\times$76 cm) with holes of 10 mm and 38 mm diameters subjected to internal pressure and far field confining stresses. As the borehole diameter increases, the

energy transferred to the surrounding rock increases. This is due to an increase of the strain energy component with increasing borehole diameter. Cuss et al. [18] obtained similar results in their experiments with sandstone.
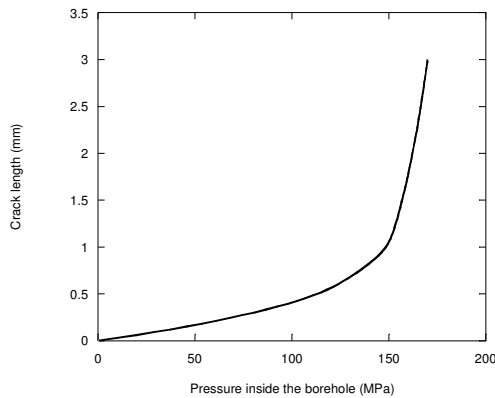

Fig. 5. Relationship between pressure inside borehole and microcrack length growth for Inada granite.

3.4. *Effect of Far-field Confining Stresses*

To investigate the effect of far-field confining pressure on the breakdown pressure, Inada granite with borehole of 50 mm diameter was simulated. The relationship between far-field confining pressure and normalized breakdown pressure for three different far-field stresses, i.e., $\sigma_{11}=\sigma_{22}=$ 10, 25 and 40 MPa are shown in Fig. 6. Note that the breakdown pressures were normalized using the reference breakdown pressure, p_r that was chosen as the breakdown pressure for the case with no far-field stresses. Increasing far-field stresses would increase the breakdown pressures which are similar to confinement effect on peak stress in triaxial compression tests.

4. Concluding Remarks

A single borehole in rock medium under internal pressure was simulated using a micromechanical continuum damage model [1].
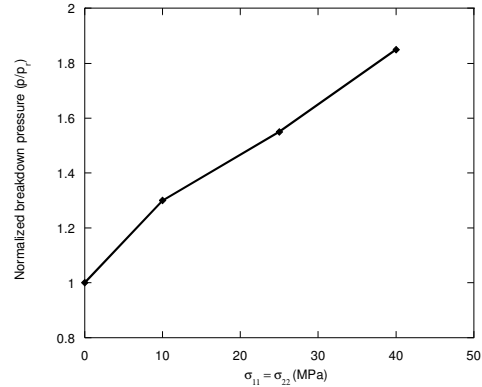
Fig. 6. Variation of breakdown pressure with far-field confining pressure for Inada granite

Numerical simulations were carried out for three types of rocks i.e., Inada granite, Mt. Isa granite and Toowoomba basalt. The model predicts that the borehole breakdown pressure and the energy transferred to the rock depend on the formation's mechanical properties, borehole size and far-field confining pressures. The modelling results show that with increasing borehole size, the energy transferred to the surrounding rock increases and the borehole breakdown pressure decreases. Furthermore, the energy seems to increase faster than the decrease of the breakdown pressure.

It should be noted that thermal energy and chemical energy were neglected in the calculation of the energy transferred to the rock around a borehole under internal pressure. For more accurate results these should be taken into consideration.

References

1. Golshani, A., Y., Okui, M., Oda and T. Takemura, 2006. A micromechanical model for brittle failure of rock and its relation to crack growth observed in triaxial compression tests of granite, *Mechanics of Materials*, 38, pp. 287–303.

2. Jaeger, J., N. G. W., Cook and R., Zimmerman, 1969, *Fundamental of rock mechanics.* Blackwell Publishing.

3. Papanastasiou, P., 1997. The influence of plasticity in hydraulic fracturing, *International Journal of Fracture*, 84, pp.61-79.

4. Griffith, A. A., 1920. The phenomena of rupture and flow in solids, *Phil. Trans. Roy. Soc. Of London*, A221, pp. 169-198.

5. Blair, S., C. and N. G. W., Cook, 1998. Analysis of compressive fracture in rock using statistical techniques: Part I. A non-linear rule-based model, *Internal Journal of Rock Mechanics and Mining Sciences*, 35, pp.837-848.

6. Costin, L. S., 1983. A microcrack model for the deformation and failure of brittle rock, *Journal of Geophysical Research*, 88, B11, pp. 9485-9492.

7. Hallbauer, D. K., H., Wagner and N. G. W., Cook, 1973. Some observations concerning the microscopic and mechanical behaviour of quartzite specimens in stiff, triaxial compression tests, *International Journal of Rock Mechanics and Mining Sciences*, 10, pp. 713-726.

8. Kranz, R. L., 1979. Crack growth and development during creep of Barre granite, *International Journal of Rock Mechanics and Mining Sciences*, 16, pp. 23-36.

9. Horii, H. and S., Nemat-Nasser, 1985a. Compression-induced microcrack growth in brittle solids: axial splitting and shear failure, *Journal of Geophysical Research*, 90, pp. 3105-3125.

10. Horii, H. and S., Nemat-Nasser, 1985b. Elastic fields of interacting inhomogeneities, *International Journal of Solid and Structures*, 21, pp. 731-745.

11. Okui, Y., H., Horii and N., Akiyama, 1993. A continuum theory for solids containing microdefects, *International Journal of Rock Mechanics & Mining Sciences & Geomechanics Abstract*s, 31, 5, pp. 735-749.

12. Nemat-Nasser, S. and M., Hori, 1993. *Micromechanics overall properties of heterogeneous materials*, North-Holland, Netherlands.

13. Takemura, T., A., Golshani, M., Oda and K., Suzuki, 2003. Preferred orientation of open microcracks in granite and their relation with anisotropic elasticity, *International Journal of Rock Mechanics and Mining Sciences*, 40, pp. 443-454.

14. Willmott, W. F., M. L., O'Flynn and N. C., Stevens, 1995. *The Bunya Mountains*, Geological Society of Australia Inc (QLD Divison).

15. Eberhardt, E., B., Stimpson and D., Stead, 1999. Effects of grain size on the initiation and propagation thresholds of stress-induced brittle failures, *Rock Mechanics and Rock Engineering*, 32, 2, pp. 81-99.

16. Guo, F., N. R., Morgenstern and J. D., Scott, 1993. Interpretation of hydraulic fracturing breakdown pressure, *International Journal of Rock Mechanics and Mining Sciences*, 30, 6, pp. 617-626.

17. Morita, N., A. D., Black and G. F., Fuh, 1996. Borehole breakdown pressure with drilling fluids-I. Empirical results, *International Journal of Rock Mechanics & Mining Sciences & Geomechanics Abstracts*, 33, pp. 39-51.

18. Cuss, R. J., E. H., Rutter and R. F., Holloway, 2003. Experimental observations of the mechanics of borehole failure in porous sandstone, *International Journal of Rock Mechanics and Mining Sciences*, 40, 747-761.